nature medicine

Hypernitrosylated ryanodine receptor calcium release channels are leaky in dystrophic muscle

Andrew M Bellinger[1], Steven Reiken[1], Christian Carlson[1], Marco Mongillo[1], Xiaoping Liu[1], Lisa Rothman[1], Stefan Matecki[2,3], Alain Lacampagne[3,4] & Andrew R Marks[1]

Duchenne muscular dystrophy is characterized by progressive muscle weakness and early death resulting from dystrophin deficiency. Loss of dystrophin results in disruption of a large dystrophin glycoprotein complex, leading to pathological calcium (Ca^{2+})-dependent signals that damage muscle cells[1–5]. We have identified a structural and functional defect in the ryanodine receptor (RyR1), a sarcoplasmic reticulum Ca^{2+} release channel, in the *mdx* mouse model of muscular dystrophy that contributes to altered Ca^{2+} homeostasis in dystrophic muscles. RyR1 isolated from *mdx* skeletal muscle showed an age-dependent increase in *S*-nitrosylation coincident with dystrophic changes in the muscle. RyR1 *S*-nitrosylation depleted the channel complex of FKBP12 (also known as calstabin-1, for calcium channel stabilizing binding protein), resulting in 'leaky' channels. Preventing calstabin-1 depletion from RyR1 with S107, a compound that binds the RyR1 channel and enhances the binding affinity of calstabin-1 to the nitrosylated channel, inhibited sarcoplasmic reticulum Ca^{2+} leak, reduced biochemical and histological evidence of muscle damage, improved muscle function and increased exercise performance in *mdx* mice. On the basis of these findings, we propose that sarcoplasmic reticulum Ca^{2+} leak via RyR1 due to *S*-nitrosylation of the channel and calstabin-1 depletion contributes to muscle weakness in muscular dystrophy, and that preventing the RyR1-mediated sarcoplasmic reticulum Ca^{2+} leak may provide a new therapeutic approach.

Duchenne muscular dystrophy (DMD), the most common X-linked disorder (affecting 1 in 3,500 male births), typically results in death as a result of respiratory or cardiac failure by age 30 (ref. 6). Loss of dystrophin leads to disruption of the dystrophin glycoprotein complex (DGC) in the sarcolemmal membrane that connects the cytoskeleton and contractile apparatus of muscle cells to the extracellular matrix and basement membrane[7,8]. Cytoplasmic calcium homeostasis in dystrophic muscle fibers is abnormal[1,3,9]. Disruption of the DGC impairs sarcolemmal membrane integrity and results in increased influx of Ca^{2+} into the muscle across the sarcolemma, which has been attributed to Ca^{2+} leak channels in the plasma membrane[5], microscopic membrane tears[3,10], mechanosensitive Ca^{2+} channels[11], or store-operated Ca^{2+} channels activated by sarcoplasmic reticulum Ca^{2+} depletion[12,13]. An elevated cytoplasmic calcium concentration ($[Ca^{2+}]_{cyt}$) is implicated in the pathophysiology of protein degradation in *mdx* muscle[4] and cell death[14]. A downstream effect of elevated $[Ca^{2+}]_{cyt}$ is activation of calpains (Ca^{2+}-dependent neutral proteases)[15]. Transgenic expression of calpastatin in the dystrophic mouse partially rescues myofiber damage[16]. It has been proposed that elevated $[Ca^{2+}]_{cyt}$ contributes to myofiber death at a rate that cannot be compensated for by recruitment of progenitor (satellite) muscle cells and regeneration and differentiation of new muscle cells[3]. Sarcoplasmic reticulum Ca^{2+} reuptake is slowed in *mdx* myofibers, and a sarcoplasmic reticulum Ca^{2+} leak of uncertain etiology has been reported[5,11,17]. The rate of Ca^{2+} sparks in dystrophic fibers is increased, further suggesting that a defect in sarcoplasmic reticulum Ca^{2+} release may be present in muscular dystrophy[18].

An approximately 80% reduction in neuronal nitric oxide synthase (nNOS) messenger RNA and protein levels has been reported in dystrophin-deficient muscle[19,20] and has been implicated in the pathophysiology of muscular dystrophy[21]. RyR1 contains multiple cysteine residues[22] that can be modified at physiological pH by either *S*-nitrosylation or *S*-glutathionylation[23–25]. Cyclic GMP–independent, nitric oxide–mediated modification of RyRs increases channel activity in single-channel measurements[22]. Exogenous *S*-nitrosylation of RyR1 has been shown to reduce the affinity of calstabin-1 binding to purified sarcoplasmic reticulum vesicles[26].

We hypothesized that defects in the macromolecular complex containing RyR1 may contribute to the abnormalities in $[Ca^{2+}]_{cyt}$ in muscular dystrophy. To test this hypothesis, we assessed the composition of the RyR1 macromolecular complex[27,28] from hind limb extensor digitorum longus (EDL) muscle of *mdx* mice. Histological evidence of muscular dystrophy is evident by 35 d of age. In mice at this age, there was a significant increase in *S*-nitrosylation of cysteine residues in RyR1 from *mdx* mice compared to age-matched wild-type (WT) littermates (**Fig. 1a**,**b**). Increased RyR1 *S*-nitrosylation correlated with depletion of calstabin-1 from the RyR1 complex (**Fig. 1a**,**b**). No differences in *S*-nitrosylation, protein kinase A (PKA) phosphorylation of RyR1 (at Ser2844) or calstabin-1 bound to the RyR1

[1]Clyde and Helen Wu Center for Molecular Cardiology, Departments of Physiology and Cellular Biophysics, and Medicine, Columbia University College of Physicians and Surgeons, 630 West 168th Street, New York, New York 10032, USA. [2]Institut National de la Santé et de la Recherche Médicale, ERI 25, F-34295 Montpellier, France. [3]Unité de Formation et de Recherche de Médecine, Université Montpellier 1, F-34295 Montpellier, France. [4]Institut National de la Santé et de la Recherche Médicale, U 637, F-34295 Montpellier, France. Correspondence should be addressed to A.R.M. (arm42@columbia.edu).

Received 2 July 2008; accepted 9 December 2008; published online 8 February 2009; doi:10.1038/nm.1916

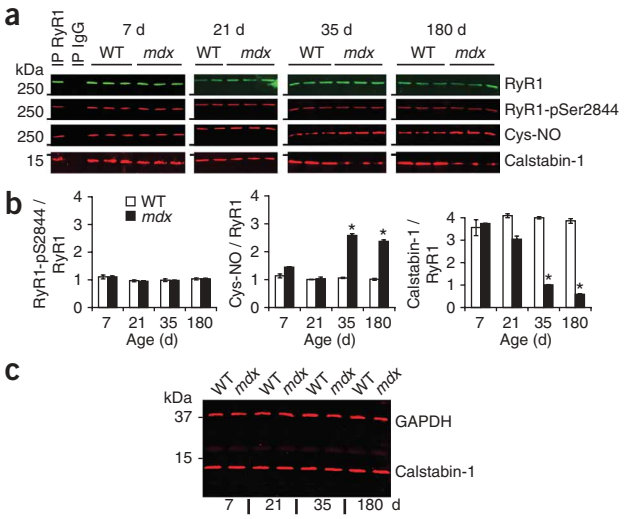

Figure 1 RyR1 is *S*-nitrosylated and depleted of calstabin-1 in *mdx* mice. (**a**) After immunoprecipitation (IP) of RyR1 from EDL muscle of *mdx* mice ($n = 3$ for each time point) and WT littermates ($n = 3$ for each time point) at 7, 21, 35 and 180 d after birth, immunoblots were used to detect total RyR1, RyR1 phosphorylated by PKA at Ser2844 (RyR1-pSer2844), *S*-nitrosylation of cysteine residues on RyR1 (Cys-NO) and calstabin-1 bound to RyR1. Positive (immunoprecipitation of RyR1 from skeletal muscle lysate) and negative (omission of antibody to RyR1; immunoprecipitation with control IgG) control immunoprecipitations were performed from 7-day-old WT skeletal muscle. Blots are representative of three independent experiments. (**b**) Quantification of the levels of PKA-phosphorylated RyR1, *S*-nitrosylated RyR1 and calstabin-1-bound to RyR1 relative to total levels of RyR1. Data are presented as means ± s.e.m. $^*P < 0.05$, *t*-test. (**c**) Immunoblot for total calstabin-1 in whole EDL muscle lysate (25 μg) from WT (n=3) and *mdx* (n=3) mice at the indicated ages. Glyceraldehyde 3-phosphate dehydrogenase (GAPDH) was used as a loading control.

complex were observed between *mdx* mice and WT littermates at 7 and 21 d of age (**Fig. 1a**,**b**). Moreover, there was no increase in PKA phosphorylation of RyR1 at Ser2844 in *mdx* mice at any age examined (**Fig. 1a**,**b**). Total amounts of calstabin-1 in whole muscle lysate were not altered in *mdx* muscle at any age, indicating that the reduced calstabin-1 binding to RyR1 is due to reduced binding to RyR1 rather than altered expression of calstabin-1 (**Fig. 1c**). Immunoprecipitation of RyR1 was specific and efficient, leaving little RyR1 in the voided fraction (**Supplementary Fig. 1** online). Thus, increased RyR1 *S*-nitrosylation and depletion of calstabin-1 correlated with muscular dystrophy in *mdx* mice.

Exogenous *S*-nitrosylation of RyR1 with nitric oxide donors resulted in depletion of calstabin-1 from the channel (**Fig. 2a**), as previously reported[26]. To identify the basis for the increased *S*-nitrosylation of RyR1, we determined the abundance of nitric oxide synthase isoforms by immunoblotting WT and *mdx* EDL muscles for inducible NOS (iNOS), endothelial NOS (eNOS) and neuronal NOS (nNOS) expression (**Fig. 2b**). iNOS amounts were significantly increased in EDL muscles from *mdx* mice 35 d and older and were essentially undetectable in WT muscle. eNOS expression was decreased in *mdx* skeletal muscle compared to WT littermates. nNOS expression was decreased in *mdx* tissue. RyR1 and iNOS (but not eNOS) co-immunoprecipitated from *mdx* EDL muscle (**Fig. 2c**,**d**), but iNOS was not detected in immunoprecipitates from WT muscle generated with antibodies to either RyR1 or iNOS (data not shown). iNOS immunoprecipitated with RyR1 at 35 and 180 d of age (**Fig. 2e**). Moreover, iNOS co-localized with RyR1 in *mdx* EDL muscle, whereas iNOS was not detected in WT EDL muscle (**Fig. 2f**). These data suggest that iNOS is a component of the RyR1 macromolecular complex in *mdx* mice, but not in WT mice.

We have reported that RyR Ca^{2+} release channel stabilizers, which we propose calling 'rycals', inhibit depletion of calstabin-1 from RyR1 hyperphosphorylated by PKA[28,29]. We hypothesized that treatment with S107, a stable, cell-permeable rycal[28], begun as early as possible in *mdx* mice, would reduce the RyR1-mediated sarcoplasmic reticulum Ca^{2+} leak induced by *S*-nitrosylation of RyR1 and calstabin-1 depletion and partially protect against muscle damage due to $[Ca^{2+}]_{cyt}$-mediated calpain activation.

We randomized 4–5-week-old male *mdx* mice into groups receiving treatment with either S107 or vehicle (H_2O) via a subcutaneous osmotic pump. After 2 weeks of treatment, forelimb grip strength was assessed. There was significant improvement in grip strength in

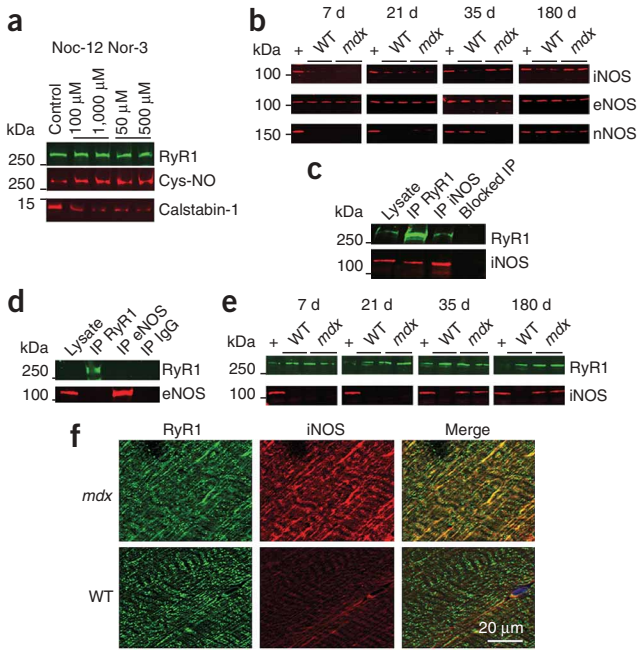

Figure 2 iNOS immunoprecipitates and co-localizes with RyR1, and *S*-nitrosylation of RyR1 depletes the channel of calstabin-1. (**a**) Immunoblot of immunoprecipitated RyR1 and bound calstabin-1 from skeletal sarcoplasmic reticulum microsomes *S*-nitrosylated *in vitro* with the NO donors Nor-3 or Noc-12. (**b**) Immunoblot showing expression of the three NOS isoforms (iNOS, eNOS and nNOS) in EDL whole-muscle lysates from WT and *mdx* mice at the indicated ages. '+' indicates positive control tissues: iNOS (mouse macrophage), eNOS (human endothelial cells) and nNOS (rat pituitary). $n = 3$ WT and *mdx* mice at each age. (**c**) RyR1 and iNOS were separately immunoprecipitated from 250 μg of *mdx* EDL muscle lysate, SDS-PAGE separated and probed for RyR1 and iNOS. 50 μg of *mdx* EDL lysate was loaded as a positive control. As a negative control, anti-RyR1 antibody was pre-incubated with a 100-fold excess antigenic peptide before immunoprecipitation (blocked IP). (**d**) Immunoprecipitation and immunoblotting of RyR1 and eNOS from *mdx* EDL lysate as in **c**. IgG negative control immunoprecipitation is also shown. (**e**) After immunoprecipitation of RyR1 from WT and *mdx* EDL lysates at the indicated ages, immunoblots were used to detect RyR1 and iNOS. '+' indicates positive controls as indicated in **b**. For **a**–**e**, data are representative of three independent experiments. (**f**) Immunohistochemistry showing colocalization of RyR1 and iNOS in mouse EDL skeletal muscle from *mdx* but not WT mice. $n = 2$ per group; representative of three or more sections from each EDL muscle.

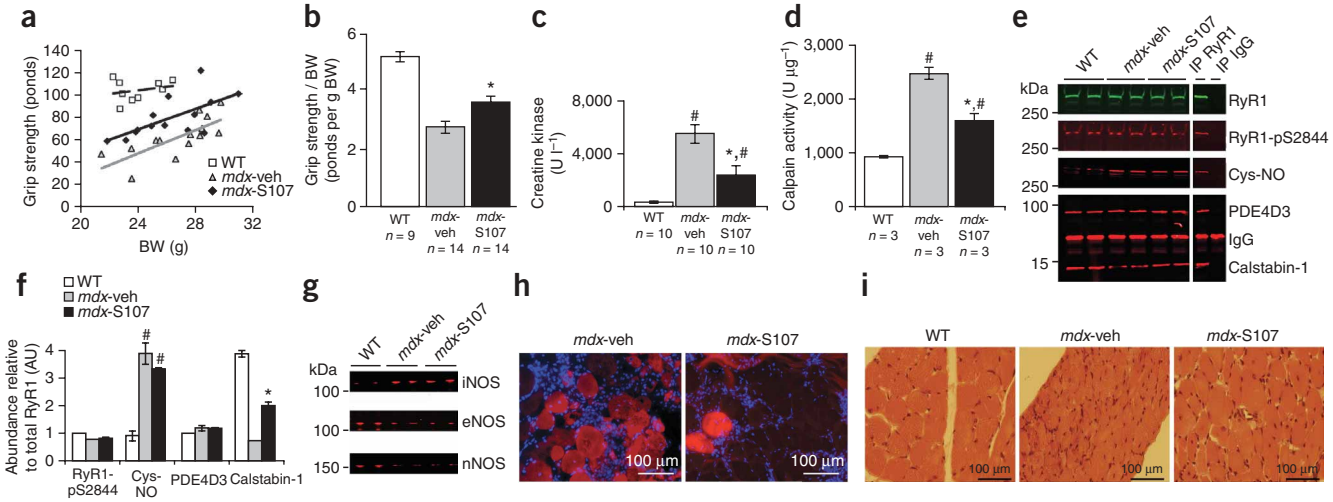

Figure 3 S107 treatment prevents calstabin-1 depletion from the RyR1 complex, improves grip strength and reduces muscle damage. (**a**) Forelimb grip strength in sedentary mice after two weeks of treatment with S107 administered via an osmotic pump (*mdx* mice given S107 (*mdx*-S107), $n = 14$) or vehicle (*mdx* mice given vehicle (*mdx*-vehicle), $n = 14$) and compared to WT mice ($n = 9$). Data are presented as a scatter plot of absolute grip strength versus body weight (BW). Least-square fit lines are overlaid. (**b**) Grip strength normalized to BW in sedentary *mdx*-S107, *mdx*-veh and WT mice. $^*P < 0.015$, *t*-test with Bonferroni adjustment, *mdx*-S107 versus *mdx*-veh. (**c**) Serum creatine kinase abundance in the same three groups of mice as in **b** ($\#P < 0.015$ versus WT; $^*P < 0.015$ *mdx*-S107 versus *mdx*-veh; *t*-tests with Bonferroni adjustment). (**d**) EDL tissue calpain activity in sedentary *mdx*-S107, *mdx*-veh and WT mice ($\#P < 0.015$ versus WT; $^*P < 0.015$ *mdx*-S107 versus *mdx*-veh; *t*-tests with Bonferroni adjustment). (**e**) After immunoprecipitation of RyR1 from EDL muscle of sedentary *mdx*-S107, *mdx*-veh and WT mice, immunoblots were used to detect total RyR1, *S*-nitrosylated RyR1 (Cys-NO), RyR1-pS2844, RyR1-bound PDE4D3 and RyR1-bound calstabin-1. (**f**) Quantification of the results in **e** showing levels of RyR1-pS2844, *S*-nitrosylated RyR1, RyR1-bound PDE4D3 and RyR1-bound calstabin-1 normalized to the total amount of RyR1. AU, arbitrary units. Data are presented as means ± s.e.m. ($\#P < 0.015$ for Cys-NO comparing *mdx* versus WT; $^*P < 0.015$ for RyR1-bound calstabin-1 for *mdx*-S107 versus *mdx*-vehicle mice). (**g**) Immunoblots for iNOS, eNOS and nNOS in EDL whole-muscle lysates from WT, *mdx*-veh, and *mdx*-S107 mice. For panels **e**–**g**, $n = 3$ mice per group. (**h**) Representative images of DAPI-stained muscle sections from Evans blue dye–injected mice to assess muscle damage in control and S107-treated mice. (**i**) Representative H&E-stained images from diaphragm of WT mice, *mdx* mice treated with vehicle or with S107 for 4 weeks as in **h**. For panels **h** and **i**, $n = 3$ or more mice per group; at least three sections from each muscle were analyzed.

the S107-treated group ($n = 14$; $P < 0.001$ versus vehicle controls ($n = 14$); **Fig. 3a**). Normalized for body weight, grip strength was significantly improved in *mdx* mice treated with S107 ($P < 0.01$ versus vehicle controls, *t*-test analysis of two independent, pair-matched and blinded cohorts; **Fig. 3b**). The serum concentration of creatine kinase, a marker of muscle necrosis, was significantly reduced by S107 treatment in *mdx* mice, suggesting a reduction in muscle damage (**Fig. 3c**). Calpain levels in EDL hind limb muscle (determined by measuring the enzymatic activity of activatable calpain in the muscle) were also reduced by S107 treatment (**Fig. 3d**), suggesting that inhibition of RyR1-mediated sarcoplasmic reticulum Ca^{2+} leak may reduce Ca^{2+}-activated proteolytic enzyme activity, leading to protection of dystrophic muscle against damage. Eccentric (lengthening) exercise such as downhill running is particularly difficult for *mdx* mice[30]. S107-treated *mdx* mice completed a 30-min downhill run at a higher rate than did vehicle-treated mice (nine of eleven mice versus three of ten, $P < 0.05$). Creatine kinase abundance was reduced in these *mdx* mice by treatment with S107 (6,200 versus 13,300 U l^{-1} in vehicle-treated *mdx* controls, $P < 0.05$), providing further evidence that S107 can improve function and reduce creatine kinase leak in *mdx* muscle. Calpain activation in EDL hind limb muscle in these *mdx* mice was reduced by S107 treatment (1,250 U μg^{-1} versus 2,100 U μg^{-1} in vehicle-treated *mdx* controls, $P < 0.05$), suggesting that stabilization of RyR1 reduced Ca^{2+} leak and Ca^{2+}-activated proteolytic enzyme activity. S107 treatment prevented depletion of calstabin-1 from *S*-nitrosylated RyR1 without affecting PKA phosphorylation of RyR1, *S*-nitrosylation of RyR1 or the levels of phosphodiesterase 4D3 (PDE4D3; **Fig. 3e**,**f**) in the RyR1 macromolecular complex. NOS isoform expression in muscle was not altered by S107 treatment (**Fig. 3g**).

Treatment of *mdx* mice with S107 via osmotic pump beginning at 4–5 weeks of age and continuing for up to 4 weeks resulted in improvement in the histological hallmarks of dystrophy. In the tibialis anterior hind limb muscle, there was a reduction in Evans blue dye–positive fibers (12.1 ± 2.8% in *mdx* mice treated with S107 ($n = 3$) versus 26.3 ± 5.3% in vehicle-treated *mdx* mice ($n = 3$, $P < 0.05$; **Fig. 3h**)). Comparison of diaphragmatic muscle from *mdx* mice treated with S107 ($n = 5$) to *mdx* mice treated with vehicle alone ($n = 4$) showed a 28% reduction in the number of central nuclei ($P < 0.05$), a 50% reduction in the number of Evans blue–positive muscle fibers ($P < 0.05$) and a 32% increase in fiber cross-sectional area ($P < 0.05$; **Fig. 3i**). These improvements in the histology of the dystrophic muscles correlated with improved muscle function and with decreased creatine kinase and calpain levels (**Fig. 3a–d**).

We subjected EDL muscle to eccentric contraction and determined the resulting force deficit, which we defined as the percentage decline in isometric force after one eccentric contraction. The decline in isometric force served as a functional indicator of contraction-induced mechanical injury to dystrophic muscle, as previously reported[30]. Force production during a tetanic contraction was recorded from EDL muscle *in situ* in anesthetized mice first in combination with an eccentric lengthening (to 115% of resting muscle length); then, after a 1-min rest, force production was recorded during a second tetanic contraction without eccentric stress (**Fig. 4a**). Eccentric contraction in *mdx* muscle resulted in a marked reduction in force production compared to control muscles (**Fig. 4b**). In mice treated for 7–10 d

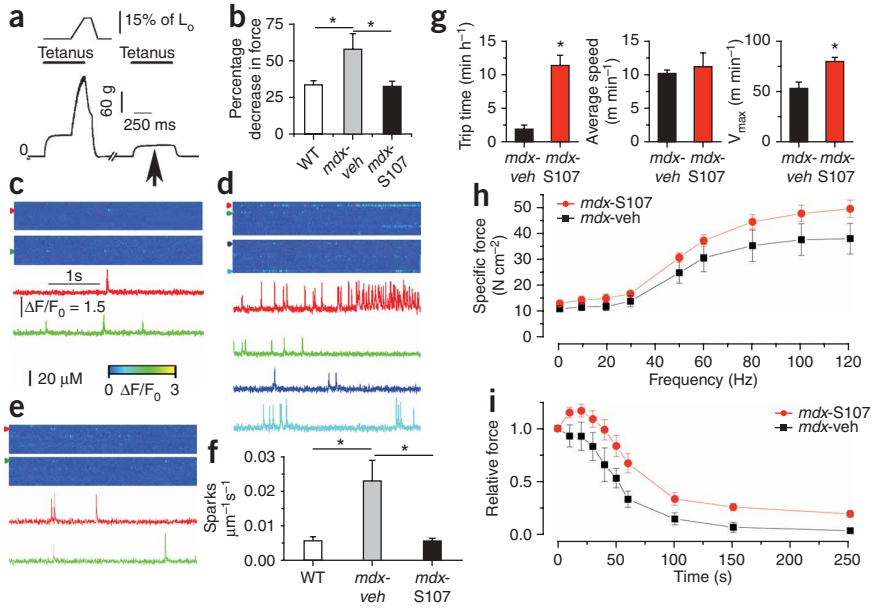

Figure 4 S107 treatment decreases Ca^{2+} leak and increases muscle force and voluntary exercise in *mdx* mice. (**a**) Isometric and eccentric force production of EDL muscle measured *in situ* in anesthetized mice, plotted as force (*y* axis) versus time (*x* axis). Top, muscle stimulation protocol. Bottom, a typical recording of force production obtained in an *mdx* mouse EDL muscle, indicating a decline in force production following the mechanical stress (arrow). L_o is the muscle length at which peak force is developed. (**b**) Quantification of the decrease in isometric force after an eccentric contraction normalized to the peak force amplitude (expressed as the percentage decrease in force) in WT control mice, vehicle-treated *mdx* mice and *mdx* mice treated with S107 (0.25 mg ml^{-1} in the drinking water administered for 10 d before testing; $n = 5$ for each group). (**c**–**e**) Spontaneous Ca^{2+} sparks recorded in WT mice (**c**), vehicle-treated *mdx* mice (**d**) and *mdx* mice treated with S107 (**e**) on the same muscles evaluated in **b**. In **c**–**e**, representative normalized fluorescence intensity ($\Delta F/F_0$) linescan images (top) from fluo-3–loaded EDL muscle fibers and the time course of fluorescence (bottom) at different locations on the linescan (colored arrowheads) are shown. Colors are arbitrary (see **Supplementary Methods** for details). Heat diagram indicates change in fluorescence as the ratio $\Delta F/F_0$. (**f**) Quantification of spark frequency in control WT mice, vehicle-treated *mdx* mice and *mdx* mice treated with S107 (three or four fibers per EDL muscle from five mice were examined for each condition; the numbers of sparks examined were 615, 2,586 and 883 in WT mice, vehicle-treated *mdx* mice and *mdx* mice treated with S107, respectively). Data are expressed as means ± s.e.m. (*$P < 0.05$ for WT versus vehicle-treated *mdx* mice or vehicle-treated *mdx* versus S107-treated *mdx* mice). (**g**) Effects of S107 treatment (0.25 mg ml^{-1} in the drinking water administered for 10 d before testing) on spontaneous physical activity of *mdx* mice. $n = 5$ mice for each condition, * $P < 0.05$. (**h**) Specific force-frequency relationship of EDL muscle from the same groups as in **g**. ($n = 5$ for each treatment group, $P < 0.001$ by a two-way analysis of variance comparing S107-treated versus vehicle-treated *mdx* mice). (**i**) EDL force during a fatigue protocol (30-Hz, 300-ms trains applied every second for 300 s). Force values are normalized to the force developed during the first train of the protocol. $n = 5$ for each treatment group, $P < 0.001$ by a two-way analysis of variance comparing S107-treated versus vehicle-treated *mdx* mice.

with S107 in their drinking water (~37.5 mg $kg^{-1}d^{-1}$), this deficit in force production after one eccentric contraction was restored to the control value (**Fig. 4b**). We thus hypothesized that impaired muscle function occurring during eccentric contractions in *mdx* mice was linked to defective RyR1 channel function, specifically to a leak of sarcoplasmic reticulum Ca^{2+} via RyR1. To further test this hypothesis, we analyzed spontaneous Ca^{2+} release events, or Ca^{2+} sparks, in EDL muscle fibers from control WT mice and in *mdx* mice after one episode of mild eccentric contraction. The Ca^{2+} spark frequency was significantly ($P < 0.05$) increased in muscle fibers from *mdx* mice compared to control mice (**Fig. 4c–f**). Other spatiotemporal properties of the sparks, including amplitude, rise time, decay time constant or spatial spread (full width at half maximum), were not different between the two groups (data not shown). Of note, there was no difference in spatiotemporal Ca^{2+} spark properties between control and *mdx* mice in the absence of mechanical stress (that is, eccentric contraction), or between control muscle with and without eccentric contraction (data not shown). Thus, inhibition of calstabin-1 depletion from the RyR1 complex by S107 treatment of *mdx* mice reduced sarcoplasmic reticulum Ca^{2+} leak via RyR1, as manifested by a reduction in Ca^{2+} spark frequency (**Fig. 4e,f**).

We next tested whether treatment with S107 could improve the voluntary exercise of *mdx* mice. After acclimating mice for 5 d to a wheel placed in their cage, we measured the length of time they spent on the wheel and their average and maximal velocities over 72 h. *Mdx* mice treated with S107 spent significantly more time on the wheel and achieved ~50% higher maximal velocities compared to *mdx* mice treated with vehicle alone (**Fig. 4g**). In addition, as determined by *in situ* force measurements of EDL muscle, S107 treatment significantly ($P < 0.001$) increased specific force (**Fig. 4h**) and resistance to fatigue (determined as relative force during repeated tetanic stimulation; **Fig. 4i**) in *mdx* muscle compared to vehicle-treated *mdx* control values.

Taken together, our data show that RyR1 Ca^{2+} release channels are leaky in *mdx* skeletal muscle owing to RyR1 hypernitrosylation, which depletes the RyR1 channel complex of the stabilizing subunit calstabin-1. Hypernitrosylation of RyR1 was associated with a marked increase in the expression of iNOS in the *mdx* muscle and formation of an iNOS-RyR1 complex. RyR1-mediated intracellular Ca^{2+} leak was associated with increased concentrations of the Ca^{2+}-activated protease calpain in *mdx* muscle that may contribute to the observed muscle damage, impaired muscle force and decreased exercise capacity in *mdx* mice. We have previously shown that calstabin-1 stabilizes the closed state of individual RyR1 channels[31] and mediates coupled gating between multiple RyR1 channels[32]. Both stabilization of the RyR1 closed state and coupled gating are likely to have roles in preventing aberrant sarcoplasmic reticulum Ca^{2+} leak through RyR1 channels. Treatment with S107, which inhibits depletion of calstabin-1 from hypernitrosylated RyR1 channels in dystrophic muscle, reduced pathological sarcoplasmic reticulum Ca^{2+} leak and calpain activation, protected against muscle damage, improved muscle force, reduced fatigue and improved grip strength and voluntary exercise in *mdx* mice.

Notably, these improvements were observed after 1 week (improved exercise capacity) or 4 weeks (histologic improvement) of S107 treatment, which is considerably faster than most genetic therapies. This suggests that the RyR1-mediated intracellular Ca^{2+} leak is downstream of the genetic defects that cause muscular dystrophy (for example, dystrophin deficiency).

It has been suggested that RyR1 channel function may be regulated by *S*-nitrosylation, but, to date, the physiological consequences of this form of regulation *in vivo* have not been well understood. nNOS is the principal source of nitric oxide in skeletal muscle. It is localized at the plasma membrane, where an N-terminal GLGF peptide motif binds to the dystrophin complex via an interaction with syntrophin[19,33]. Disruption of the DGC in DMD results in a selective loss of nNOS catalytic activity that is associated with its downregulation at the transcriptional level[19,20]. Recently, decreased abundance of sarcolemmal-localized nNOS was shown to be linked to vasoconstriction and decreased physical activity after mild exercise (10-min downhill run) in mouse models including *mdx* mice, and treatment with a PDE5 inhibitor increased physical activity after mild exercise[34]. In contrast, iNOS expression is substantially increased in the skeletal muscle of both humans with DMD and *mdx* mice, and rescue of the *mdx* phenotype by adenoviral-mediated dystrophin or utrophin expression normalizes iNOS activity[35]. The concurrent downregulation of nNOS and upregulation of iNOS suggests that the latter could be a compensatory response. However, functional compensation may be precluded by differences in the subcellular localization of the two NOS isoforms. In muscular dystrophy, both the effects of increased nitrosative stress on the RyR1 complex and increased Ca^{2+} influx across the plasma membrane due to disruption of the DGC may activate RyR1 channels. Depletion of the stabilizing subunit calstabin-1 (FKBP12) from the RyR1 channel due to nitrosative stress may render it particularly sensitive to Ca^{2+}-mediated activation.

Therapeutic strategies for muscular dystrophy include gene therapy to replace dystrophin[36], upregulation of the dystrophin homolog utrophin[37], acceleration of the rate of muscle regeneration[38,39] and exon skipping achieved via virus-mediated expression of antisense sequences linked to a modified U7 small nuclear RNA[40]. Stabilization of RyR1 by inhibiting sarcoplasmic reticulum Ca^{2+} leak with a small molecule may provide an additional strategy to protect against muscle damage and improve function.

METHODS

Mice and treatment with S107. We obtained C57BL/10ScSc-Dmd^{mdx}/J mice, referred to as *mdx* mice (stock number 001801) and C57BL/6J mice, referred to as WT mice, from Jackson Laboratories and bred them to obtain male *mdx* and WT littermate controls. We randomized the mice to groups receiving treatment with either S107 (for additional information on synthesis and specificity, see **Supplementary Methods** online and ref. 28) or vehicle (H_2O). In some experiments, we subcutaneously implanted osmotic pumps (Alzet model 1004, 100 µl total volume, 0.11 µl h^{-1} delivery for ~28 d, Durect) filled with H_2O or S107 (80 µg µl^{-1} diluted in H_2O) on the dorsal surface of each mouse by a horizontal incision at the neck for 2–4 weeks as indicated in the legend to **Figure 3**. In other experiments, we added S107 to the drinking water (final concentration, 0.25 mg ml^{-1}) as indicated in the legend to **Figure 4**. The mice drank ~3 ml per day (water consumption was variable, and we recorded water bottle and body weight to monitor consumption) for a daily dose of ~0.75 mg (~37.5 mg kg^{-1} d^{-1}), which resulted in a plasma S107 concentration of ~35 ± 21 ng ml^{-1} (~140 nM, which we determined in the early morning to reflect higher water consumption during the night). We conducted all experiments in accordance with protocols approved by the Institutional Animal Care and Use Committees of Columbia University and Université Montpellier. All studies involving drug treatments, including analyses of function and histologic sections, were conducted by individuals blinded to the treatment status of the mice.

Immunoblotting. Membranes were incubated for 1–2 h at room temperature with primary antibody to RyR1 (RyR1-1327, an affinity-purified rabbit polyclonal antibody raised against a KLH-conjugated peptide with the amino acid sequence CAEPDTDYENLRRS, corresponding to residues 1327–1339 of mouse skeletal RyR1, with an additional cysteine residue added to the amino terminus), and affinity purified with the unconjugated peptide. This antibody specifically recognizes RyR1, as it does not react with RyR2 or RyR3 when used at a 1 in 2,500 or 1 in 5,000 dilution for immunoblotting and at a 1 in 250 dilution for immunoprecipitation (data not shown). We also used antibody to calstabin (1 in 2,500 in blocking buffer, LICOR Biosciences); phospho-epitope–specific antibody to human RyR2 phosphorylated on Ser2809 (1 in 5,000)[41], which detects PKA-phosphorylated mouse RyR1 (on Ser2844) and RyR2 (on Ser2808); antibody to *S*-nitrosylated cysteine residues (1 in 1,000, Sigma); antibody to PDE4D3 (1 in 1,000)[42]; and antibodies to iNOS (1 in 2,000, VWR), eNOS (1 in 2,000, VWR) and nNOS (1 in 1,000, VWR). For additional biochemical methods, including *S*-nitrosylation of RyR1 with Nor-3 and Noc-12, see **Supplementary Methods**.

Grip strength. We assessed forelimb grip strength after two weeks of treatment with S107 or vehicle. We allowed each mouse to grab a hold bar attached to a force transducer that records the peak force generated as the mouse is pulled by the tail horizontally away from the bar (model number 303500-M/C-1, TSE Systems). We performed five consecutive pulls separated by 15-s pauses between each pull. We calculated the absolute grip strength as the average of the peak forces recorded from the middle three pulls (in ponds, 1 pond = ~9.8 mN), and a normalized grip strength, which is the absolute grip strength divided by the body weight in grams.

Creatine kinase and calpain assay. We determined creatine kinase levels on the basis of absorbance change per minute by a commercial assay according to the manufacturer's instructions (Pointe Scientific). We diluted EDL muscle homogenates to a final concentration of 600 µg ml^{-1}, and we determined the calpain activity in the homogenate with a commercial assay according to the manufacturer's instructions (Calbiochem).

Measurement of extensor digitorum longus resistance to contraction-induced mechanical stress. We anesthetized mice (male, 40 d old) with 130 mg kg^{-1} ketamine and 20 mg kg^{-1} xylazine and immobilized them in the supine position on a surgical platform at 37 °C. We exposed the anterior region of the lower hind limb from the ankle to just above the knee and dissected free the distal tendons of the tibialis anterior and EDL. We tied the distal tendon of the EDL with a 4–0 nylon suture to the lever arm of a force transducer and length servomotor system (model 305B dual mode; Aurora Scientific), which was mounted on a mobile micrometer stage to allow fine incremental adjustments of muscle length. We kept the exposed muscles moist with a 37 °C isotonic saline drip. We stimulated the EDL indirectly via an electrode placed on the belly of the tibialis anterior. For details of the stimulation protocols, see **Supplementary Methods**.

Calcium sparks. We acquired fluorescence images with a Zeiss LSM 510 META NLO confocal system equipped with a three-point 63× water immersion objective (numerical aperture = 1.2) operated in line-scan mode (1.5 ms per line, 3,000 lines per scan) along the longitudinal axis of the fibers. We excited Fluo-3 at 488 nm with an Argon laser and recorded the emitted fluorescence at 525 nm. Additional details of spark measurement are in the **Supplementary Methods**.

Voluntary exercise measurements. We evaluated voluntary exercise in mice by placing a 5.5-cm-wide by 12-cm diameter wheel in a 15 cm × 40 cm × 15 cm cage.

Statistical analysis. We presented data as means ± s.e.m. We used an independent *t*-test with a significance level of 0.05 to test differences between *mdx* and WT mice. When we made multiple comparisons between WT mice, *mdx* mice treated with vehicle and *mdx* mice treated with S107, we used a Bonferroni adjustment with a pair-wise significance level of 0.015.

Note: Supplementary information is available on the Nature Medicine website.

ACKNOWLEDGMENTS

This work was supported in part by a grant from the Leducq Foundation. We thank J. Shan for assistance with analyses of histologic sections and J. Fauconnier for help with voluntary exercise measurements in mice.

AUTHOR CONTRIBUTIONS
A.M.B. conducted experiments and wrote the manuscript, S.R. performed biochemistry experiments, C.C. assisted with mouse experiments, M.M. performed immunohistochemistry, X.L. and L.R. assisted with histology, S.M. and A.L. performed muscle and calcium experiments, and A.R.M. conceived, designed and directed the project, analyzed data and wrote the final version of the manuscript.

COMPETING INTERESTS STATEMENT
The authors declare competing financial interests: details accompany the full-text HTML version of the paper at http://www.nature.com/naturemedicine/.

Published online at http://www.nature.com/naturemedicine/
Reprints and permissions information is available online at http://npg.nature.com/reprintsandpermissions/

1. Bodensteiner, J.B. & Engel, A.G. Intracellular calcium accumulation in Duchenne dystrophy and other myopathies: a study of 567,000 muscle fibers in 114 biopsies. *Neurology* **28**, 439–446 (1978).
2. Glesby, M.J., Rosenmann, E., Nylen, E.G. & Wrogemann, K. Serum CK, calcium, magnesium, and oxidative phosphorylation in *mdx* mouse muscular dystrophy. *Muscle Nerve* **11**, 852–856 (1988).
3. Blake, D.J., Weir, A., Newey, S.E. & Davies, K.E. Function and genetics of dystrophin and dystrophin-related proteins in muscle. *Physiol. Rev.* **82**, 291–329 (2002).
4. Turner, P.R., Westwood, T., Regen, C.M. & Steinhardt, R.A. Increased protein degradation results from elevated free calcium levels found in muscle from *mdx* mice. *Nature* **335**, 735–738 (1988).
5. Fong, P.Y., Turner, P.R., Denetclaw, W.F. & Steinhardt, R.A. Increased activity of calcium leak channels in myotubes of Duchenne human and *mdx* mouse origin. *Science* **250**, 673–676 (1990).
6. Hoffman, E.P., Brown, R.H. & Kunkel, L.M. Dystrophin: the protein product of the duchenne muscular dystrophy locus. *Cell* **51**, 919–928 (1987).
7. Bonilla, E. *et al.* Duchenne muscular dystrophy: Deficiency of dystrophin at the muscle cell surface. *Cell* **54**, 447–452 (1988).
8. Matsumura, K., Ervasti, J.M., Ohlendieck, K., Kahl, S.D. & Campbell, K.P. Association of dystrophin-related protein with dystrophin-associated proteins in *mdx* mouse muscle. *Nature* **360**, 588–591 (1992).
9. Yeung, E.W. *et al.* Effects of stretch-activated channel blockers on $[Ca^{2+}]_i$ and muscle damage in the mdx mouse. *J. Physiol. (Lond.)* **562**, 367–380 (2005).
10. Bradley, W.G. & Fulthorpe, J.J. Studies of sarcolemmal integrity in myopathic muscle. *Neurology* **28**, 670–677 (1978).
11. Franco, A., Jr. & Lansman, J.B. Calcium entry through stretch-inactivated ion channels in *mdx* myotubes. *Nature* **344**, 670–673 (1990).
12. Vandebrouck, C., Martin, D., Colson-Van Schoor, M., Debaix, H. & Gailly, P. Involvement of TRPC in the abnormal calcium influx observed in dystrophic (*mdx*) mouse skeletal muscle fibers. *J. Cell Biol.* **158**, 1089–1096 (2002).
13. Boittin, F.-X. *et al.* Ca^{2+}-independent phospholipase A2 enhances store-operated Ca^{2+} entry in dystrophic skeletal muscle fibers. *J. Cell Sci.* **119**, 3733–3742 (2006).
14. Robert, V. *et al.* Alteration in calcium handling at the subcellular level in *mdx* myotubes. *J. Biol. Chem.* **276**, 4647–4651 (2001).
15. Spencer, M.J., Croall, D.E. & Tidball, J.G. Calpains are activated in necrotic fibers from *mdx* dystrophic mice. *J. Biol. Chem.* **270**, 10909–10914 (1995).
16. Spencer, M.J. & Mellgren, R.L. Overexpression of a calpastatin transgene in *mdx* muscle reduces dystrophic pathology. *Hum. Mol. Genet.* **11**, 2645–2655 (2002).
17. Turner, P.R., Fong, P.Y., Denetclaw, W.F. & Steinhardt, R.A. Increased calcium influx in dystrophic muscle. *J. Cell Biol.* **115**, 1701–1712 (1991).
18. Wang, X. *et al.* Uncontrolled calcium sparks act as a dystrophic signal for mammalian skeletal muscle. *Nat. Cell Biol.* **7**, 525–530 (2005).
19. Brenman, J.E., Chao, D.S., Xia, H., Aldape, K. & Bredt, D.S. Nitric oxide synthase complexed with dystrophin and absent from skeletal muscle sarcolemma in Duchenne muscular dystrophy. *Cell* **82**, 743–752 (1995).
20. Chang, W.J. *et al.* Neuronal nitric oxide synthase and dystrophin-deficient muscular dystrophy. *Proc. Natl. Acad. Sci. USA* **93**, 9142–9147 (1996).
21. Wehling, M., Spencer, M.J. & Tidball, J.G. A nitric oxide synthase transgene ameliorates muscular dystrophy in mdx mice. *J. Cell Biol.* **155**, 123–131 (2001).
22. Xu, L., Eu, J.P., Meissner, G. & Stamler, J.S. Activation of the cardiac calcium release channel (ryanodine receptor) by poly-*S*-nitrosylation. *Science* **279**, 234–237 (1998).
23. Sun, J., Xin, C., Eu, J.P., Stamler, J.S. & Meissner, G. Cysteine-3635 is responsible for skeletal muscle ryanodine receptor modulation by NO. *Proc. Natl. Acad. Sci. USA* **98**, 11158–11162 (2001).
24. Aracena, P., Sanchez, G., Donoso, P., Hamilton, S.L. & Hidalgo, C. *S*-glutathionylation decreases Mg^{2+} inhibition and *S*-nitrosylation enhances Ca^{2+} activation of RyR1 channels. *J. Biol. Chem.* **278**, 42927–42935 (2003).
25. Sun, J., Xu, L., Eu, J.P., Stamler, J.S. & Meissner, G. Nitric oxide, NOC-12, and *S*-nitrosoglutathione modulate the skeletal muscle calcium release channel/ryanodine Receptor by different mechanisms. An allosteric function for O_2 in *S*-nitrosylation of the channel. *J. Biol. Chem.* **278**, 8184–8189 (2003).
26. Aracena, P., Tang, W., Hamilton, S. & Hidalgo, C. Effects of *S*-glutathionylation and *S*-nitrosylation on calmodulin binding to triads and FKBP12 binding to type 1 calcium release channels. *Antioxid. Redox Signal.* **7**, 870–881 (2005).
27. Marx, S.O. *et al.* Phosphorylation-dependent regulation of ryanodine receptors: a novel role for leucine/isoleucine zippers. *J. Cell Biol.* **153**, 699–708 (2001).
28. Bellinger, A. *et al.* Remodeling of ryanodine receptor complex causes "leaky" channels: a molecular mechanism for decreased exercise capacity. *Proc. Natl. Acad. Sci. USA* **105**, 2198–2202 (2008).
29. Wehrens, X.H. *et al.* Enhancing calstabin binding to ryanodine receptors improves cardiac and skeletal muscle function in heart failure. *Proc. Natl. Acad. Sci. USA* **102**, 9607–9612 (2005).
30. Vilquin, J.T. *et al.* Evidence of *mdx* mouse skeletal muscle fragility in vivo by eccentric running exercise. *Muscle Nerve* **21**, 567–576 (1998).
31. Brillantes, A.B. *et al.* Stabilization of calcium release channel (ryanodine receptor) function by FK506-binding protein. *Cell* **77**, 513–523 (1994).
32. Marx, S.O., Ondrias, K. & Marks, A.R. Coupled gating between individual skeletal muscle Ca^{2+} release channels (ryanodine receptors). *Science* **281**, 818–821 (1998).
33. Kameya, S. α1-syntrophin gene disruption results in the absence of neuronal-type nitric-oxide synthase at the sarcolemma but does not induce muscle degeneration. *J. Biol. Chem.* **274**, 2193–2200 (1999).
34. Kobayashi, Y.M. *et al.* Sarcolemma-localized nNOS is required to maintain activity after mild exercise. *Nature* **456**, 511–515 (2008).
35. Louboutin, J.P., Rouger, K., Tinsley, J.M., Halldorson, J. & Wilson, J.M. iNOS expression in dystrophinopathies can be reduced by somatic gene transfer of dystrophin or utrophin. *Mol. Med.* **7**, 355–364 (2001).
36. Gregorevic, P. *et al.* rAAV6-microdystrophin preserves muscle function and extends lifespan in severely dystrophic mice. *Nat. Med.* **12**, 787–789 (2006).
37. Krag, T.O.B. *et al.* Heregulin ameliorates the dystrophic phenotype in mdx mice. *Proc. Natl. Acad. Sci. USA* **101**, 13856–13860 (2004).
38. Zaccagnini, G. *et al.* $p66^{ShcA}$ and oxidative stress modulate myogenic differentiation and skeletal muscle regeneration after hindlimb ischemia. *J. Biol. Chem.* **282**, 31453–31459 (2007).
39. Khurana, T.S. & Davies, K.E. Pharmacological strategies for muscular dystrophy. *Nat. Rev. Drug Discov.* **2**, 379–390 (2003).
40. Goyenvalle, A. *et al.* Rescue of dystrophic muscle through U7 snRNA-mediated exon skipping. *Science* **306**, 1796–1799 (2004).
41. Marx, S.O. *et al.* PKA phosphorylation dissociates FKBP12.6 from the calcium release channel (ryanodine receptor): defective regulation in failing hearts. *Cell* **101**, 365–376 (2000).
42. Reiken, S. *et al.* PKA phosphorylation activates the calcium release channel (ryanodine receptor) in skeletal muscle: defective regulation in heart failure. *J. Cell. Biol.* **160**, 919–928 (2003).